Published in final edited form as:

Neurobiol Aging. 2016 April ; 40: 173–180. doi:10.1016/j.neurobiolaging.2016.01.133.

β-amyloid, hippocampal atrophy and their relation to longitudinal brain change in cognitively normal individuals

Evan Fletcher, Ph.D[1], **Sylvia Villeneuve, Ph.D**[2], **Pauline Maillard, Ph.D**[1], **Danielle Harvey, Ph.D**[3], **Bruce Reed, Ph.D**[1], **William Jagust, MD**[4], and **Charles DeCarli, MD**[1]

Sylvia Villeneuve: villeneuve.sylvia@gmail.com; Pauline Maillard: pauli.maillard@gmail.com; Danielle Harvey: djharvey@phs.ucdavis.edu; Bruce Reed: brread@ucdavis.edu; William Jagust: jagust@berkeley.edu; Charles DeCarli: charles.decarli@ucdmc.ucdavis.edu

[1]Department of Neurology, University of California at Davis, Davis, CA, USA

[2]Douglas Mental Health University Institute, McGill University, Montreal, Canada

[3]Division of Biostatistics, School of Medicine, University of California at Davis, Davis, CA, USA

[4]Helen Wills Neuroscience Institute, University of California, Berkeley, Berkeley CA, USA

Abstract

Recent literature has examined baseline hippocampal volume and extent of brain amyloidosis to test potential synergistic effects on worsening cognition and extent of brain atrophy. Use of hippocampal volume in prior studies was based on the notion that limbic circuit degeneration is an early manifestation of the Alzheimer's Disease (AD) pathophysiology. To clarify these interactions early in the AD process, we tested the effects of amyloid and baseline normalized hippocampal volume on longitudinal brain atrophy rates in a group of cognitively normal individuals. Results showed that the combination of elevated β-amyloid and baseline hippocampal atrophy is associated with increased rates specific to the limbic circuit and splenium. Importantly, this atrophy pattern emerged from a voxelwise analysis, corroborated by regression models over ROIs in native space. The results are broadly consistent with previous studies of the effects of amyloid and baseline hippocampal atrophy in normals, while pointing to accelerated atrophy of AD-vulnerable regions detectable at the preclinical stage.

Corresponding Author: Evan Fletcher, Center for Neuroscience, 1544 Newton Court, Davis, California 95616, evanfletcher@gmail.com, Office phone: 530 757-8585, Fax : 530 757-8827.

Author contributions: Fletcher: Background research, study design, data analysis, manuscript writing
Villeneuve: Study design, data generation, data analysis, manuscript editing
Maillard: Data analysis
Harvey: Data analysis
Reed: Study design, data generation
Jagust: Data generation, manuscript editing
DeCarli: Study design, data generation, data analysis, manuscript editing

Authors report no conflicts of interest and no disclosures.

Keywords

Alzheimer's; longitudinal; atrophy; β-amyloid; neurodegeneration; normals

Introduction

The occurrence of β-amyloidosis and tauopathy in trajectories of brain aging and cognitive decline has been laid out in sequential models(Jack and Holtzman, 2013, Jack, et al., 2010) of β-amyloid deposition followed by elevated tau and then macrostructural atrophy. Recent studies have focused on baseline hippocampal volume and brain hypometabolism in interaction with β-amyloidosis as predictors of brain atrophy(Jack, et al., 2014, Kantarci, et al., 2014) or cognitive decline(Mormino, et al., 2014, Wirth, et al., 2013). In these articles baseline hippocampal volume and brain hypometabolism are used as markers for a process labeled “neurodegeneration” that is independent of β-amyloidosis (Jack, et al., 2014). This process may consist of “primary age-related tauopathy” (PART)(Crary, et al., 2014, Jack, 2014) and on its own may lead to “suspected non-Alzheimer's pathology” (SNAP)(Jack, 2014) in the absence of β-amyloidosis. The presence of both conditions, however, may lead to accelerated brain change and cognitive decline. For instance, previous studies have shown that the co-occurrence of neurodegeneration and β-amyloid accelerates the rate of cognitive decline in older adults(Mormino, et al., 2014, Wirth, et al., 2013). Recent research has also highlighted that β-amyloid can increase or catalyze neurodegeneration so that individuals with both processes show a greater rate of brain atrophy than those with only neurodegeneration or only β-amyloid(Jack, et al., 2014); similar findings have also recently been made for decreased white matter integrity(Kantarci, et al., 2014).

The limbic circuit(Thomas, et al., 2011) appears to be an early target of AD degeneration(Acosta-Cabronero and Nestor, 2014) as measured both by medial temporal gray matter atrophy(Ishii, et al., 2005) and FDG-PET hypometabolism in medial temporal gray as well as posterior cingulate(Nestor, et al., 2003). It includes projections from the hippocampus via the fornix to the mammillary bodies, through portions of the thalamus to the posterior cingulate (PC), and is completed by projections from the PC back to the presubicular regions of the hippocampus(Nestor, et al., 2003). The mechanisms of this circuit-wide degeneration are not yet clear. Hippocampal degeneration may be an indicator of this process, but in the light of findings cited above it is possible that the presence of *both* low baseline hippocampal volume and high amyloidosis is necessary to predict limbic degeneration.

To clarify these questions, we tested the hypothesis that baseline hippocampal volume interacts with β-amyloidosis to predict accelerated longitudinal tissue loss in a cohort of normal older study participants. We performed a voxel-based analysis to test for effects throughout the brain, followed by ROI-based analyses in order to better localize and confirm the effects of these factors and their interactions on atrophy of the brain.

Methods

Participants

Our longitudinal cohort consisted of 53 normal (CN) participant recruited into the Longitudinal Cohort of the Alzheimer's Disease Center (ADC) of the University of California, Davis. Our sample was drawn from a group of available participants having PiB imaging as part of an ongoing image database acquisition at the ADC. Each participant received two structural MRI scans at intervals no more closely spaced than 8 months with an average interscan interval of 3.8 years, as well as a clinical diagnosis performed at or near each scan date. Each participant also received a single PiB scan within an average interval of 2.7 years from the baseline MRI, or 1.1 years before the follow-up scan.

Clinical Evaluation

Clinical evaluations were performed by the ADC at baseline and follow up visits. These included detailed medical history and physical and neurological examinations. Diagnoses of cognitive symptoms were made according to standardized criteria(McKhann, et al., 2011, Mungas, et al., 2011, Petersen, 2004) by a consensus of clinicians.

Magnetic Resonance Imaging

Each participant received two scans on a scanner of the same manufacturer and model at both occasions to minimize artifact differences in longitudinal registrations. The mean interval between successive scans was 3.8 years. All images were acquired at the Imaging Research Center of the University of California, Davis. The scanners had field strengths of 1.5T and 3T. The 1.5T GE Genesis Signa had the following parameters: Scan type FSPGR, flip angle 15°, TR 8.9 ms, field of view 25 cm, slice thickness 1.5 mm. The 3T Siemens Trio had the following parameters: Scan type MPRAGE, flip angle 7°, TR 2500 ms, field of view 25cm, slice thickness 1.5 mm.

Biomarkers

All PiB-PET images were acquired at Lawrence Berkeley National Laboratory (LBNL) on a Siemens ECAT EXACT HR PET scanner in 3D acquisition mode. PiB radiotracer was synthesized at this facility using a standard protocol(Mathis, et al., 2003) 10 to 15 mCi of [^{11}C] PiB was injected into an antecubital vein. Dynamic acquisition frames (34 to 35 frames total) were obtained over 90 minutes as follows: 4 × 15 seconds, 8 × 30 seconds, 9 × 60 seconds, 2 × 180 seconds, 8 × 300 or 10 × 300 seconds and 3 × 600 or 2 × 600 seconds. Distribution volume ratio (DVR) images were created with PiB frames corresponding to 35-90 minutes post-injection and a gray matter cerebellar mask as reference region(Logan, et al., 1996, Price, et al., 2005). Cerebellar gray matter was chosen as the reference because it is known to be relatively unaffected by fibrillar amyloid in AD and is thus reliable for estimating non-specific PiB binding(Price, et al., 2005).

For each participant, a global direct value ratio (DVR) index was derived from the native-space image(Villeneuve, et al., 2014) by averaging the weighted mean value from freesurfer-derived ROIs in frontal (cortical regions anterior to the precentral gyrus), temporal (middle and superior temporal regions), parietal (supramarginal gyrus, inferior/

superior parietal lobules and precuneus) and posterior cingulate cortex using the Desikan-Killiany atlas(Desikan, et al., 2006).

For a categorical measure of PiB index, we used a cutoff at 1.08 which represents an optimal cutoff in our laboratory to detect early PiB signal when using the processing method describe above(Villeneuve, et al., 2015). PiB index values below this cutoff were classified as amyloid-negative (A-); otherwise amyloid positive (A+).

Brain PiB loads were measured at dates such that the mean time difference between PiB measurement and baseline MRI scan was 2.72 years. PiB load was considered as constant over the interscan interval of each participant. This was justified because of the known slow rate of PiB increase from healthy controls to AD, spanning decades, with a further plateauing at higher levels(Villemagne, et al., 2013).

Hippocampal volume was computed by a semi-automatic multi-atlas hippocampal segmentation algorithm(Aljabar, et al., 2009). Hippocampal volumes were regressed against total brain volume and residuals, i.e. adjusted hippocampal volume (HVa) used as unbiased indicators (Jack, et al., 2012). We define hippocampal atrophy (HA) as the negative residual of the baseline hippocampal volume after regression against brain size, i.e. HA = -HVa. Thus higher values of HA suggest smaller hippocampal volumes. To create a categorical measure from HA we applied a threshold for HVa derived from the 90^{th} percentile of HVa in an independent group of AD participants (Jack, et al., 2012): values below this threshold were termed hippocampal-atrophy positive (HA+), otherwise negative (HA-). Therefore HA + refers to low baseline hippocampal volume (below the AD percentile cutoff) and HA-to high.

In our main analysis we used continuous versions of both PiB and HA. However, for comparison with previous studies(Jack, et al., 2014, Kantarci, et al., 2014) we also refer to the four biomarker groups A-HA-, A+HA-, A-HA+ and A+HA+ in one of our analyses and our demographic table.

Longitudinal change analysis

Voxelwise longitudinal change between same-participant T1 structural MRIs was computed using a tensor-based morphometry (TBM) method designed to enhance sensitivity and specificity by incorporating knowledge of likely tissue boundary locations(Fletcher, 2014, E Fletcher, et al., 2013). Prior to TBM registration, the two scans of each participant were denoised using a non-local means algorithm optimized for structural brain T1 images(Coupé, et al., 2008). This algorithm takes advantage of image redundancy to robustly model tissue intensities and smooth regions within tissues while preserving edges(Buades, et al., 2005). Brain change was quantified at the voxel level by the TBM deformation field at each voxel. In this analysis, the determinant of the 3×3 derivative matrix of the deformation field at a voxel computes the local volume change factor indicated by the deformation. Determinants equal to 1.0 indicate no volume change; determinants between 0 and 1 signify volume shrinkage, while determinants greater than 1.0 indicate expansion. Performing a logarithmic transform gives a symmetric distribution about 0, with negative logs indicating contraction and positive logs indicating expansion(E Fletcher, et al.,

2013, Hua, et al., 2008). These will be referred to as log-jacobians. To perform group voxelwise statistical analysis in a common space, native space log-jacobians were transformed onto a minimal deformation template (MDT) adapted to an older population(Kochunov, et al., 2001), using parameters derived from affine alignment followed by non-linear B-spline warping(Rueckert, et al., 2006) of the underlying structural T1 images. The individual log-jacobians in template space were annualized to represent change over the same interscan time interval in all participants. To compensate for the matching variability of the B-spline warps and improve voxelwise statistical power in template space, an intensity-consistent smoothing(Studholme and Cardenas, 2002) was performed on each participant's warped jacobian image after deformation to the template. In this approach, weights for the jacobian values are computed based on estimates of the likelihood that nearby locations originated from the same tissue in native space. The resulting neighborhood weighted averages offer improved edge preservation in the template space and decreased “dilution” when, for example, contractive jacobians are improperly averaged with expansions, due to misregistrations committed by the B-spline warps(Studholme and Cardenas, 2002).

Statistical analysis

Voxel-based group comparisons—To assess possible relations between PiB, HA and brain tissue loss without prior hypothesis as to location, we performed multivariate voxel-based regression using the log-jacobian images transformed to template space. We controlled for age and gender while testing for effects of continuous PiB, continuous HA and their interaction on log-jacobian change. To correct for multiple voxel comparisons, contiguous cluster significance was assessed by non-parametric sub-threshold cluster testing(Nichols and Holmes, 2001) with 1000 iterations of random permutations, creating a distribution of maximal voxel cluster sizes for t-values above or below threshold depending upon the effect under evaluation, then retaining clusters in the original regression t-images (one for each effect) whose size was above the top 95^{th} percentile in the distributions of maximal cluster sizes from the permutations. This significance permutation testing was done for clusters from three separate thresholds of t magnitudes 2.0, 2.5 and 3.0 (with signs appropriate to the effects, here all negative because increasing PiB, HA and their product all lead to greater tissue loss) to assess differences in the strengths of the effects over the brain.

ROI-based analysis—We next performed regression analyses for mean log-jacobian values over ROIs in participant native space. ROI selection was by the extent of overlap between the significant clusters in template space and regions known to exhibit atrophy or change for participants in the Alzheimer's trajectory(Braak and Braak, 1996, Chételat, et al., 2013, Fletcher, et al., 2014, Kantarci, et al., 2014, Nestor, et al., 2003). We retained those whose overlap was at least 15% of their volume in template space. ROIs on this list were reverse transformed to each participant native brain and the mean values of annualized log-jacobians there were used in multi-regression models to analyze the effects of continuous PiB, continuous HA and their interaction on tissue change. To eliminate possible overlap in native space of transformed ROIs due to imprecision of the spline deformations, we used a “voting” scheme to assign native voxels to the highest probability among all deformed ROIs or none of our list in native space. For each ROI, we evaluated models predicting log-

jacobian ROI means involving HA. Let *n* denote HA, *p* denote PiB and Y the ROI mean log-jacobian change. Then our regression model of log-jacobian change is expressed as

$$Y=\beta_0+\beta_1 p+\beta_2 n+\beta_3 pn.$$

If the product coefficient β_3 is nonzero, the slope of the change in Y with respect to one variable is altered when holding the other variable at a fixed value. For example, a fixed PiB value and a nonzero β_3 alter the slope of change with respect to HA according to the formula:

$$Y=(\beta_0+\beta_1 p_{fixed})+(\beta_2+\beta_3 p_{fixed})n$$

in which (β_2 + β_3 p_{fixed}) is the new slope for the effect of *n*. Similarly for the reverse. The regression model involving two continuous variables and their product can only support a symmetrical interpretation of the contributions of *p* and *n* because β_3 applies to both factors in the product term. To study possible difference in the effects of *p* and *n* we also introduced asymmetry, using regression models in which one variable was categorical (with n_{cat} or p_{cat} present or absent, say p_{cat} = 1 or 0 for *p* above or below the PiB cutoff) with the other one continuous. In these models one can visualize the difference in slope of change for the continuous variable with and without the presence of the categorical. For example, if PiB is categorical (the model with p_{cat} and continuous *n*), the slope of change of *Y* with respect to *n* is either β_2 (in the population where p_{cat} = 0) or β_2 + β_3 (in the population where p_{cat} =1).

ROIs in template space were created in-house or adapted from well-known atlases. The Brodmann ROIs were generated in-house by an experienced neurologist and have been used in previous publications from our laboratory(Evan Fletcher, et al., 2013, Lee, et al., 2012). Hippocampal ROIs were computed in native space by a multi-atlas based automatic segmentation method(Aljabar, et al., 2009). Tissue compartments in each ROI were obtained from a 4-tissue segmentation of the native space MRI, using a Bayesian maximal-likelihood algorithm enhanced for sensitivity at tissue boundaries(Fletcher, et al., 2012).

Results

Participant characteristics

Characteristics of the normal cohort are displayed in Table 1. There were 53 participants with a mean age of 74.0 years, standard deviation 7.35. Gender distribution was 51% male. Mean interscan interval (ΔScan = date 2 – baseline date) was 3.8 years, with median 2.7 years and 75th percentile 5.7 years. The mean DVR (brain PiB index) was 1.17 with standard deviation 0.23. The mean interval between baseline scan date and PiB acquisition date (ΔPiB = PiB date – baseline date) was 2.72 years. The range of this difference was -2.15 to 9.67 years, with the median being 2.0 years and 75th percentile being 4.5 years. Cognitive scores of CDR and MMSE were close to expected values for normal participants and changed little from baseline to date 1, with the exception of the biomarker-positive

group A+HA+ whose CDR scores were larger and showed more than a two-fold increase at the second scan. From Table 1, there were 23 PiB+ and 23 HA+ participants.

Voxel-based analysis

For an overview of atrophy rates in our normal cohort we calculated average log-jacobians after normalizing interscan intervals to two years (Fig. 1). There were loss rates of 2-3% in the genu of the corpus callosum, thalamus, caudate and neighboring periventricular areas, portions of the cingulum and portions of the insula and the frontal cortices (Fig. 1), along with changes of 1-2% in the splenium (Fig. 1, left) and gray matter regions of the temporal lobes (Fig. 1, right). Next we tested for voxel-based multi-regressions effects of continuous PiB, continuous HA and their interaction on log-jacobian change, controlling for age and gender. There were no significant clusters at thresholds of t magnitude 2.0 or higher for separate effects of PiB or HA in either set of models. However we found significant clusters of effects for their interaction at t-magnitude thresholds of 2.0, 2.5, 3.0, 3.5 and 4.0. Significant clusters for these interaction effects in template space are displayed in Fig. 2. The figures suggest that the strongest correlations of tissue loss with PiB × HA occurred posteriorly and medially, in and around the splenium and posterior cingulate cortex.

Analyzing our composite significant clusters for overlaps with ROIs relevant to change in AD, we selected ROIs having overlaps of at least 15% of their volumes with significant clusters for PiB × HA of threshold $t > 2.5$. The maps of these ROI overlaps are shown in Fig. 3.

ROI-based analysis with continuous HA and PiB

For ROI-based models we chose ROIs having overlap > 15% with significant clusters of threshold $t > 2.5$ in our voxel analyses (see previous section), plus the hippocampus and entorhinal areas (Brodmann 28 and 34) because these are implicated in early stages of AD. Results are displayed in Table 2 for models involving continuous PiB, HA and their interactions. The six ROIs yielded a total of 18 hypotheses to check for family-wise error (i.e. at each ROI, the p-values for each single effect of PiB, HA and for PiB × HA). We controlled for FWER < 0.05. Checking FWER for these hypotheses showed that the PiB × HA effect survived for the splenium (starred entry in Table 2). Among the individual ROI tests the splenium, posterior cingulate (BA 23), and retrosplenial cortex (BA 26-29) had interaction effects with $p < 0.05$, significant for their model (bold). Additionally, hippocampal atrophy showed a significant individual effect of PiB and the posterior cingulate a significant single effect of HA.

To test whether generalized gray matter atrophy, as opposed to hippocampal volume, has an effect on longitudinal atrophy rates, we repeated each of the analyses of Table 2 adding total cortical gray matter volume, adjusted by regression against whole brain size, as a covariate. This variable was never significant in itself and resulted in marginal changes of the p-values for other effects. Of the effects in bold in Table 2, only that for the retrosplenial cortex (BA 26-29) went from significant ($p = 0.0359$) to trending at $p = 0.07$ with the addition of cortical gray matter. And for BA 34, the effect of HA which was previously trending became barely significant at $p = 0.0419$. In view of the variability both in ΔScan and ΔPiB,

we also repeated the regressions of Table 2 adding these as covariates. In every ROI, the overall model fit was improved only marginally if at all. ΔScan was significant only in the model of PiB and HA over splenium, while ΔPiB was never significant. Finally, the pattern of significance for PiB, HA and their interaction was the same in every case, including survival after FWER correction.

ROI-based models with one categorical and one continuous variable

To further visualize the interactions of PiB and HA, we performed a third set of regressions on change in the splenium, making PiB and HA each categorical in turn while holding the remaining variable continuous. As in the previous regressions, log-jacobians were residuals after controlling for age and gender. As discussed previously, PiB cutoff was set to 1.08. The cutoff threshold for HA was the 90th percentile of adjusted hippocampal volume (HVa) in an independent cohort of AD participants, equal to -0.24 in our AD cohort. HA+ comprised HVa values below this threshold (recall HA = -HVa). The resulting biomarker subgroup sizes are shown in Table 1. Results of each model are graphed in Fig. 4 with splenium atrophy vs. continuous PiB in high and low HA subgroups (left) and vs. continuous HA in high and low PiB subgroups (right). In the left panel there is very little relation between continuous PiB DVR and splenium atrophy in the low HA (blue) but a strong negative correlation in the high HA (red). A similar set of relations is seen in the right panel.

Discussion

We investigated the hypotheses that PiB, baseline hippocampal volume or their interactions predict longitudinal brain atrophy rates in our normal cohort. An overview of atrophy rates indicated group average losses in gray and white matter areas consistent with known patterns of normal aging (Fig. 1). Strong losses in cortical gray confirm that the TBM method is capable of picking up anatomically localized GM changes. We then analyzed associations of atrophy with our biomarkers in voxel and ROI-based regression models. Significant voxel clusters of association with PiB × HA occurred extensively in posterior regions overlapping a large portion of the splenium as well the posterior cingulate and retrosplenial cortex (RSC) (Figs 2, 3). Areas of strongest association between PiB × HA and atrophy were generally different than areas of greatest average atrophy over the cohort (compare Figs. 1 and 2). ROI-based regressions confirmed the significance of these ROIs in separate models (Table 2). The splenium additionally survived FWER < 0.05. There were further individual associations of PiB with hippocampal atrophy, and HA with posterior cingulate atrophy (Table 2). Separate regressions involving continuous PiB with categorical HA, and the reverse, reinforced the hypothesis that interaction of the two factors is significant for atrophy rates in the splenium (Fig. 4).

These regions have been previously implicated in the Alzheimer's trajectory of brain changes(Acosta-Cabronero, et al., 2010, Catheline, et al., 2010, Nestor, et al., 2003, Wang, et al., 2006). The hippocampus, posterior cingulate and RSC are components of the “limbic-diencephalic” circuit that appears to be an early target of AD degeneration(Acosta-Cabronero and Nestor, 2014, Nestor, et al., 2003). These components tend to decline in

concert(Ishii, et al., 2005, Nestor, et al., 2003), and DTI studies have indicated that white matter tracts connecting them also suffer early vulnerability and decline(Acosta-Cabronero, et al., 2010). Reduced WM integrity in the posterior cingulum has been identified as a marker of early AD, contrasted with anterior cingulum decline as a marker of normal aging (Catheline, et al., 2010). A volumetric study of ROIs specific to this region, BA 23, 29 and 30, showed that the extent of atrophy there was similar to the extent hippocampal atrophy among a group with incipient AD, concluding that these regions may be specifically vulnerable to AD pathology(Pengas, et al., 2010). We have previously reported that in a cognitively normal cohort, longitudinal atrophy rates in the splenium, RSC and posterior cingulate ROIs were correlated with reduced FA measure of WM integrity in the fornix(Fletcher, et al., 2014). The splenium consists of connections to the posterior cingulate and retrosplenial areas (i.e. BA 23, 29 and 30), as well as to primary visual and sensory areas(Putnam, et al., 2010). Volume measurements of the splenium find significant reductions, relative to normal controls, among normal participants with cognitive complaints, MCI and AD(Wang, et al., 2006), and reduced FA in AD compared to MCI(Mielke, et al., 2009). Conversely, the splenium is more robust against the effects of normal aging and hypertension than more anterior portions of the corpus callosum(Burgmans, et al., 2010). This may help explain why splenium atrophy rates were the most strongly associated of any ROI with PiB × HA (Table 2) even though group average splenium atrophy was modest, less for example than in the genu (Fig. 1).

Our present results among cognitively normal participants suggest that low hippocampal volume in combination with elevated brain amyloid is strongly associated with accelerated atrophy rates in posterior regions including the splenium and posterior components of the limbic circuit. The strong effects of PiB × HA interaction are consistent with previous recent results regarding the synergistic effects of amyloid and “neurodegeneration”(Jack, et al., 2014, Kantarci, et al., 2014). They also parallel recent research implicating amyloid × neurodegeneration in cognitive decline among normals(Mormino, et al., 2014), suggesting that such early cognitive decline may correspond to brain injury from increased atrophy rates catalyzed by PiB × HA. Future research will test this hypothesis directly. Consideration of the biomarker models of amyloid and tau (Jack and Holtzman, 2013) may also suggest the hypothesis that accelerated atrophy rates are catalyzed by interaction of amyloidosis and tauopathy. This is consistent with our results, substituting HA for tauopathy, but the involvement of tauopathy cannot be confirmed with our dataset. It awaits a study with larger sample size that includes tau imaging.

Limitations

Although for each participant both MRI scans were done on the same scanner, different scanner models were represented among all the participants in our available dataset. Similarly, a range of intervals between MRI and PET acquisitions resulted from limitations in our dataset. The variability in ΔPiB and in ΔScan could challenge the assumption of constant PiB over the participant scan intervals. Even so, the repetition of regressions with and without these variables revealed little appreciable change, suggesting that the interaction effects we found are robust to this variability. Another limitation is the small sample size, roughly one-fifth or less of the other recent studies cited above for normal cohorts (Jack, et

al., 2014, Kantarci, et al., 2014). This may have hindered the sensitivity to statistical effects, especially for single effects of PiB or HA. That being said, our results for interaction effects are robust and broadly consistent with those studies, and this provides validation for the present study. There may also be a limitation related to the capabilities of the TBM method used. For example, despite edge enhancement and intensity-consistent smoothing, it is difficult to pick up significant localized changes in small structures like the fornix or hippocampus that are bordered by CSF regions. Our results may therefore understate changes in these structures. Finally, individual variation in cortical topography and resulting mismatches when deforming to template image may have weakened statistical power to pick up significant associations in cortical gray regions. We have attempted to compensate for this possibility by our post-hoc intensity consistent smoothing of log-jacobian images in template space (Studholme, et al., 2003). Nonetheless, our results may understate the significance of GM region associations.

Conclusion

In a normal cohort, the combination of β-amyloid and baseline normalized hippocampal volume is associated with increased rates of longitudinal tissue loss in specific regions that overlap areas known to be vulnerable early in the Alzheimer's trajectory, including the splenium and posterior portions of the limbic circuit. These regions emerged from a voxelwise template-space analysis and were corroborated by regression models over ROIs in native space. Neither amyloid nor baseline hippocampal volume showed large effects without the other. The results are broadly consistent with previous studies of the effects of amyloid and HA in normals, while specifically linking accelerated atrophy of AD-vulnerable limbic and splenium regions to the interactions of amyloid and HA. These atrophy patterns are detectable at an early preclinical stage.

Acknowledgments

This work was supported by the following grants:

P30 AG10129 DeCarli (PI)

R01 AG021028 DeCarli (PI)

R01 AG047827 DeCarli (PI)

References

Acosta-Cabronero J, Nestor PJ. Diffusion tensor imaging in Alzheimer's disease: insights into the limbic-diencephalic network and methodological considerations. Frontiers in aging neuroscience. 2014; 6:266.10.3389/fnagi.2014.00266 [PubMed: 25324775]

Acosta-Cabronero J, Williams GB, Pengas G, Nestor PJ. Absolute diffusivities define the landscape of white matter degeneration in Alzheimer's disease. Brain : a journal of neurology. 2010; 133:529–39.10.1093/brain/awp257 [PubMed: 19914928]

Aljabar P, Heckemann Ra, Hammers a, Hajnal JV, Rueckert D. Multi-atlas based segmentation of brain images: atlas selection and its effect on accuracy. NeuroImage. 2009; 46:726–38.10.1016/j.neuroimage.2009.02.018 [PubMed: 19245840]

Braak H, Braak E. Evolution of the neuropathology of Alzheimer's disease. Acta Neurologica Scandinavica. 1996; 94:3–12.10.1111/j.1600-0404.1996.tb05866.x [PubMed: 8740983]

Buades A, Coll B, Morel JM. A Review of Image Denoising Algorithms, with A New One. Multiscale Modeling & Simulation. 2005; 4:490–530.

Burgmans S, van Boxtel MPJ, Gronenschild EHBM, Vuurman EFPM, Hofman P, Uylings HBM, Jolles J, Raz N. Multiple indicators of age-related differences in cerebral white matter and the modifying effects of hypertension. NeuroImage. 2010; 49:2083–93.10.1016/j.neuroimage.2009.10.035 [PubMed: 19850136]

Catheline G, Periot O, Amirault M, Braun M, Dartigues JF, Auriacombe S, Allard M. Distinctive alterations of the cingulum bundle during aging and Alzheimer's disease. Neurobiology of Aging. 2010; 31:1582–92.10.1016/j.neurobiolaging.2008.08.012 [PubMed: 18829135]

Chételat G, Landeau B, Salmon E, Yakushev I, Bahri MA, Mézenge F, Perrotin A, Bastin C, Manrique A, Scheurich A, Scheckenberger M, Desgranges B, Eustache F, Fellgiebel A. Relationships between brain metabolism decrease in normal aging and changes in structural and functional connectivity. NeuroImage. 2013; 76:167–77.10.1016/j.neuroimage.2013.03.009 [PubMed: 23518010]

Coupé P, Yger P, Prima S, Hellier P, Kervrann C. An Optimized Blockwise Non Local Means Denoising Filter for 3D Magnetic Resonance Images An Optimized Blockwise Non Local Means Denoising Filter for 3D Magnetic Resonance Images. IEEE transactions on medical imaging. 2008; 27:425–41. [PubMed: 18390341]

Crary JF, Trojanowski JQ, Schneider Ja, Abisambra JF, Abner EL, Alafuzoff I, Arnold SE, Attems J, Beach TG, Bigio EH, Cairns NJ, Dickson DW, Gearing M, Grinberg LT, Hof PR, Hyman BT, Jellinger K, Jicha Ga, Kovacs GG, Knopman DS, Kofler J, Kukull Wa, Mackenzie IR, Masliah E, McKee A, Montine TJ, Murray ME, Neltner JH, Santa-Maria I, Seeley WW, Serrano-Pozo A, Shelanski ML, Stein T, Takao M, Thal DR, Toledo JB, Troncoso JC, Vonsattel JP, White CL, Wisniewski T, Woltjer RL, Yamada M, Nelson PT. Primary age-related tauopathy (PART): a common pathology associated with human aging. Acta Neuropathologica. 2014; 128:755–66.10.1007/s00401-014-1349-0 [PubMed: 25348064]

Desikan RS, Ségonne F, Fischl B, Quinn BT, Dickerson BC, Blacker D, Buckner RL, Dale AM, Maguire RP, Hyman BT, Albert MS, Killiany RJ. An automated labeling system for subdividing the human cerebral cortex on MRI scans into gyral based regions of interest. NeuroImage. 2006; 31:968–80.10.1016/j.neuroimage.2006.01.021 [PubMed: 16530430]

Fletcher, E. Using Prior Information To Enhance Sensitivity of Longitudinal Brain Change Computation. In: Chen, CH., editor. Frontiers of Medical Imaging. World Scientific; 2014. p. 63-81.

Fletcher E, Carmichael O, Pasternak O, Maier-Hein KH, DeCarli C. Early Brain Loss in Circuits Affected by Alzheimer's Disease is Predicted by Fornix Microstructure but may be Independent of Gray Matter. Frontiers in Aging Neuroscience. 2014; 6:1–9.10.3389/fnagi.2014.00106 [PubMed: 24478697]

Fletcher E, Knaack a, Singh B, Lloyd E, Wu E, Carmichael O, Decarli C. Combining Boundary-Based Methods with Tensor-Based Morphometry in the Measurement of Longitudinal Brain Change. IEEE transactions on medical imaging. 2013; 32(2):223–36.10.1109/TMI.2012.2220153 [PubMed: 23014714]

Fletcher E, Raman M, Huebner P, Liu A, Mungas D, Carmichael O, Decarli C. Loss of Fornix White Matter Volume as a Predictor of Cognitive Impairment in Cognitively Normal Elderly Individuals. JAMA Neurology. 2013; 95616:1–7.10.1001/jamaneurol.2013.3263

Fletcher E, Singh B, Harvey D, Carmichael O, DeCarli C. Adaptive image segmentation for robust measurement of longitudinal brain tissue change. 2012 Annual International Conference of the IEEE Engineering in Medicine and Biology Society. 2012:5319–22.10.1109/EMBC.2012.6347195

Hua X, Leow A, Parikshak N, Lee S, Chiang M, Toga A, Jackjr C, Weiner M, Thompson P. Tensor-based morphometry as a neuroimaging biomarker for Alzheimer's disease: An MRI study of 676 AD, MCI, and normal subjects. NeuroImage. 2008; 43(3):458–69.10.1016/j.neuroimage.2008.07.013 [PubMed: 18691658]

Ishii K, Sasaki H, Kono AK, Miyamoto N, Fukuda T, Mori E. Comparison of gray matter and metabolic reduction in mild Alzheimer's disease using FDG-PET and voxel-based morphometric MR studies. European journal of nuclear medicine and molecular imaging. 2005; 32:959–63.10.1007/s00259-004-1740-5 [PubMed: 15800784]

Jack CR. PART and SNAP. Acta neuropathologica. 2014; 128:773–6.10.1007/s00401-014-1362-3 [PubMed: 25380757]

Jack, Clifford R.; Holtzman, David M. Biomarker Modeling of Alzheimer's Disease. Neuron. 2013; 80:1347–58.10.1016/j.neuron.2013.12.003 [PubMed: 24360540]

Jack CR, Knopman DS, Jagust WJ, Shaw LM, Aisen PS, Weiner MW, Petersen RC, Trojanowski JQ. Hypothetical model of dynamic biomarkers of the Alzheimer's pathological cascade. Lancet neurology. 2010; 9:119–28.10.1016/S1474-4422(09)70299-6 [PubMed: 20083042]

Jack CR, Knopman DS, Weigand SD, Wiste HJ, Vemuri P, Lowe V, Kantarci K, Gunter JL, Senjem ML, Ivnik RJ, Roberts RO, Rocca Wa, Boeve BF, Petersen RC. An operational approach to National Institute on Aging-Alzheimer's Association criteria for preclinical Alzheimer disease. Annals of neurology. 2012; 71:765–75.10.1002/ana.22628 [PubMed: 22488240]

Jack CR, Wiste HJ, Knopman DS, Vemuri P, Mielke MM, Weigand SD, Senjem ML, Gunter JL, Lowe V, Gregg BE, Pankratz VS, Petersen RC. Rates of β-amyloid accumulation are independent of hippocampal neurodegeneration. Neurology. 2014; 82:1605–12.10.1212/WNL.0000000000000386 [PubMed: 24706010]

Kantarci K, Schwarz CG, Reid RI, Przybelski Sa, Lesnick TG, Zuk SM, Senjem ML, Gunter JL, Lowe V, Machulda MM, Knopman DS, Petersen RC, Jack CR. White Matter Integrity Determined With Diffusion Tensor Imaging in Older Adults Without Dementia: Influence of Amyloid Load and Neurodegeneration. JAMA neurology. 201410.1001/jamaneurol.2014.1482

Kochunov P, Lancaster JL, Thompson P, Woods R, Mazziotta J, Hardies J, Fox P. Regional Spatial Normalization: Toward and Optimal Target. Journal of Computer Assisted Tomography. 2001; 25(5):805–16. [PubMed: 11584245]

Lee D, Fletcher E, Carmichael O, Singh B, Mungas D, Reed BR, Martinez O, Buonocore M, Persianinova M, Decarli C. Sub-regional hippocampal injury is associated with fornix degeneration in Alzheimer's disease. Frontiers in Aging Neuroscience. 2012; 4:1–10.10.3389/fnagi.2012.00001 [PubMed: 22514534]

Logan J, Fowler JS, Volkow ND, Wang GJ, Ding YS, Alexoff DL. Distribution volume ratios without blood sampling from graphical analysis of PET data. Journal of cerebral blood flow and metabolism : official journal of the International Society of Cerebral Blood Flow and Metabolism. 1996; 16:834–40.10.1097/00004647-199609000-00008

Mathis, Ca; Mathis, Ca; Wang, YM.; Wang, YM.; Holt, DP.; Holt, DP.; Huang, GF.; Huang, GF.; Debnath, ML.; Debnath, ML.; Klunk, WE.; Klunk, WE. Synthesis and evaluation of C-11-labeled 6-substituted 2-arylbenzothiazoles as amyloid imaging agents. J Med Chem. 2003; 46:2740–54. [PubMed: 12801237]

McKhann GM, Knopman DS, Chertkow H, Hyman BT, Jack CR, Kawas CH, Klunk WE, Koroshetz WJ, Manly JJ, Mayeux R, Mohs RC, Morris JC, Rossor MN, Scheltens P, Carrillo MC, Thies B, Weintraub S, Phelps CH. The diagnosis of dementia due to Alzheimer's disease: Recommendations from the National Institute on Aging-Alzheimer's Association workgroups on diagnostic guidelines for Alzheimer's disease. Alzheimer's and Dementia. 2011; 7:263–9.10.1016/j.jalz.2011.03.005

Mielke MM, Kozauer Na, Chan KCG, George M, Toroney J, Zerrate M, Bandeen-Roche K, Wang MC, Vanzijl P, Pekar JJ, Mori S, Lyketsos CG, Albert M. Regionally-specific diffusion tensor imaging in mild cognitive impairment and Alzheimer's disease. NeuroImage. 2009; 46:47–55.10.1016/j.neuroimage.2009.01.054 [PubMed: 19457371]

Mormino EC, Betensky Ra, Hedden T, Schultz AP, Amariglio RE, Rentz DM, Johnson Ka, Sperling Ra. Synergistic Effect of β-Amyloid and Neurodegeneration on Cognitive Decline in Clinically Normal Individuals. JAMA Neurology. 2014; 71:1379.10.1001/jamaneurol.2014.2031 [PubMed: 25222039]

Mungas D, Beckett L, Harvey D, Farias ST, Carmichael O, Olichney J, Miller J, Decarli C. Heterogeneity of Cognitive Trajectories in Diverse Older Person. Psychology and Aging. 2011; 25:606–19.10.1037/a0019502.Heterogeneity [PubMed: 20677882]

Nestor PJ, Fryer TD, Smielewski P, Hodges JR. Limbic hypometabolism in Alzheimer's disease and mild cognitive impairment. Annals of neurology. 2003; 54:343–51.10.1002/ana.10669 [PubMed: 12953266]

Nichols T, Holmes AP. Nonparametric permutation tests for functional neuroimaging: a primer with examples. Human Brain Mapping. 2001; 15(1):1–25. [PubMed: 11747097]

Pengas G, Hodges JR, Watson P, Nestor PJ. Focal posterior cingulate atrophy in incipient Alzheimer's disease. Neurobiology of Aging. 2010; 31:25–33.10.1016/j.neurobiolaging.2008.03.014 [PubMed: 18455838]

Petersen RC. Mild cognitive impairment as a diagnostic entity. Journal of Internal Medicine. 2004; 256:183–94.10.1111/j.1365-2796.2004.01388.x [PubMed: 15324362]

Price JC, Klunk WE, Lopresti BJ, Lu X, Hoge Ja, Ziolko SK, Holt DP, Meltzer CC, DeKosky ST, Mathis Ca. Kinetic modeling of amyloid binding in humans using PET imaging and Pittsburgh Compound-B. Journal of cerebral blood flow and metabolism : official journal of the International Society of Cerebral Blood Flow and Metabolism. 2005; 25:1528–47.10.1038/sj.jcbfm.9600146

Putnam MC, Steven MS, Doron KW, Riggall AC, Gazzaniga MS. Cortical projection topography of the human splenium: hemispheric asymmetry and individual differences. Journal of cognitive neuroscience. 2010; 22:1662–9.10.1162/jocn.2009.21290 [PubMed: 19583478]

Rueckert D, Aljabar P, Heckemann RA, Hajnal JV, Hammers A, Larsen R, Nielsen M, Sporring J. Diffeomorphic registration using b-splines. MICCAI 2006 LNCS. 2006; 4191:702–9.

Studholme C, Cardenas V. An intensity consistent approach to the cross sectional analysis of deformation tensor derived maps of brain shape. … Image Computing and …. 2002:492–9.

Studholme C, Cardenas V, Maudsley A, Weiner M. An intensity consistent filtering approach to the analysis of deformation tensor derived maps of brain shape. NeuroImage. 2003; 19(4):1638–49.10.1016/s1053-8119(03)00183-6 [PubMed: 12948718]

Thomas AG, Koumellis P, Dineen Ra. The fornix in health and disease: an imaging review. Radiographics : a review publication of the Radiological Society of North America, Inc. 2011; 31:1107–21.10.1148/rg.314105729

Villemagne VL, Burnham S, Bourgeat P, Brown B, Ellis Ka, Salvado O, Szoeke C, Macaulay SL, Martins R, Maruff P, Ames D, Rowe CC, Masters CL. Amyloid β deposition, neurodegeneration, and cognitive decline in sporadic Alzheimer's disease: a prospective cohort study. Lancet neurology. 2013; 12:357–67.10.1016/S1474-4422(13)70044-9 [PubMed: 23477989]

Villeneuve S, Rabinovici GD, Cohn-sheehy BI, Madison C, Ayakta N, Ghosh PM, Joie RL, Arthur-bentil SK, Vogel JW, Marks SM, Lehmann M, Rosen HJ, Reed B, Olichney J, Boxer AL, Miller BL, Borys E, Jin Lw, Huang EJ, Grinberg LT, Decarli C, Seeley WW, Jagust W. Existing Pittsburgh Compound-B positron emission tomography thresholds are too high : statistical and pathological evaluation. Brain : a journal of neurology. 2015:1–14.10.1093/brain/awv112 [PubMed: 25564487]

Villeneuve S, Reed BR, Madison CM, Wirth M, Marchant NL, Kriger S, Mack WJ, Sanossian N, DeCarli C, Chui HC, Weiner MW, Jagust WJ. Vascular risk and Ab interact to reduce cortical thickness in AD vulnerable brain regions. Neurology. 2014; 83:40–7.10.1212/WNL.0000000000000550 [PubMed: 24907234]

Wang PJ, Saykin AJ, Flashman La, Wishart Ha, Rabin La, Santulli RB, McHugh TL, MacDonald JW, Mamourian AC. Regionally specific atrophy of the corpus callosum in AD, MCI and cognitive complaints. Neurobiology of aging. 2006; 27:1613–7.10.1016/j.neurobiolaging.2005.09.035 [PubMed: 16271806]

Wirth M, Oh H, Mormino EC, Markley C, Landau SM, Jagust WJ. The effect of amyloid β on cognitive decline is modulated by neural integrity in cognitively normal elderly. Alzheimer's and Dementia. 2013; 9:687–98.10.1016/j.jalz.2012.10.012

Highlights

- Effects of β-amyloid, neurodegeneration on brain degeneration remain unclear
- In normals, their interaction is associated with increased longitudinal atrophy
- Highest association areas overlap key circuits vulnerable to Alzheimer's pathology
- Overlaps include posterior components of default mode network and limbic circuit
- Preclinical AD-signature atrophy from interaction of amyloid, neurodegeneration.
- Detectability of these early effects may be valuable for biomarker intervention

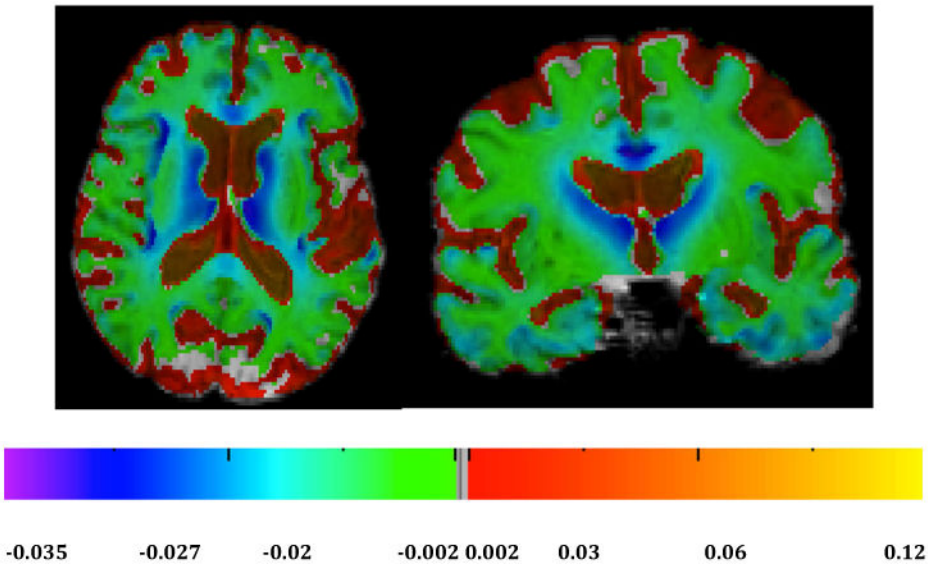

Fig. 1.

Average log-jacobians for normal cohort. Left: axial. Right: coronal. Color bars indicate magnitude changes (approximately % change) over normalized two-year period.

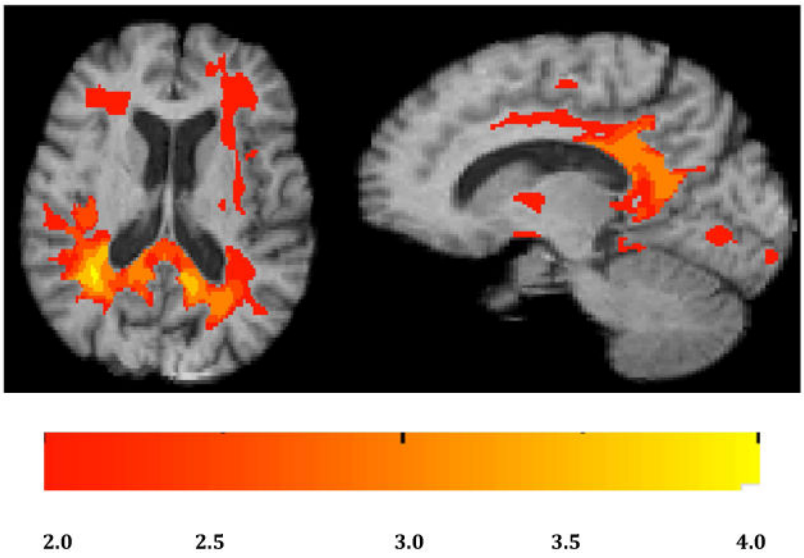

Fig. 2.

Significant clusters of association for PiB × HA vs. log-jacobian tissue change. Left: axial. Right: sagittal. Color bar indicates magnitude of t-values for significant clusters.

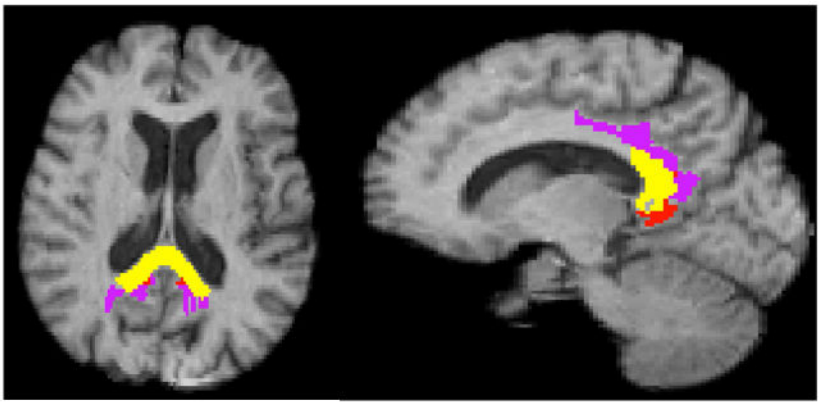

Fig. 3.

ROI overlaps with significant clusters of Fig. 1. Overlaps with clusters of significant interaction PiB × HA, t > 2.5. Yellow: splenium. Purple, posterior cingulum (Brodmann 23); Red: retrosplenial cortex (Brodmann 26-29).

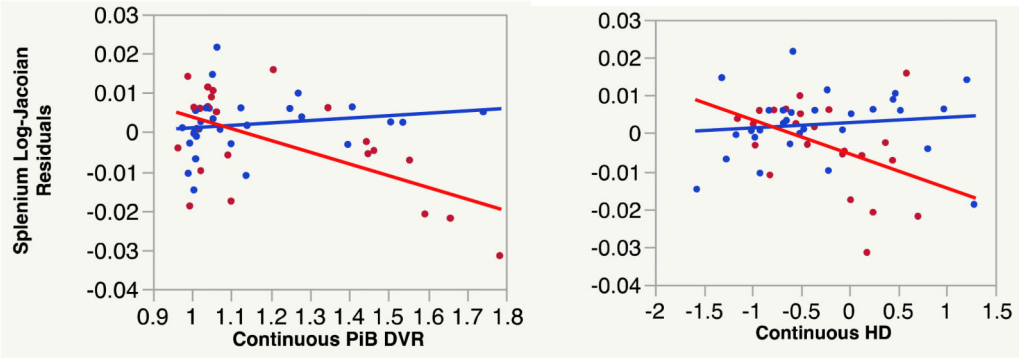

Fig. 4.

Plots of multi-regression models involving categorical HA with continuous PiB (left) and categorical PiB with continuous HA (right). Blue and red show data for low and high HA, respectively, plotted against continuous PiB (left) and low and high PiB, respectively, plotted against continuous HA (right). Regression lines show the relation of splenium log-jacobians in each category for the corresponding continuous variable. Log-jacobians are residuals after controlling for age and gender. Categorical cutoffs: for PiB, 1.08; for HA, -0.24.

Table 1

Average characteristics by biomarker group Abbreviations: A±: amyloid positive or negative; HA±: hippocampal degeneration positive or negative. See text for definitions of cutoffs. CDR: CDR sum of boxes scores, at baseline and follow up times. Similarly for MMSE. PiB –Baseline: average time interval between PiB imaging and baseline scan (positive means PiB acquisition was later).

Biomarker Category	N	Interscan Interval (Years)	PiB – Baseline (Years)	CDR1	CDR2	MMSE1	MMSE2
A-HA-	18	3.82	3.09	0.56	0.42	28.3	28.1
A+HA-	12	4.07	3.08	0.50	0.71	28.7	28.2
A-HA+	12	3.76	2.04	0.29	0.75	29.0	28.0
A+HA+	11	3.49	2.50	0.73	1.68	28.4	26.9
All Normals	53	3.80	2.73	0.52	0.82	28.6	27.9

Table 2

Summary of models showing the effects of continuous PiB and continuous HA for log-jacobian mean atrophy rates over specified ROIs. Individual model regression test significant effects are bold. Single star indicates further significance at FWER <= 0.05. Abbreviations: BA 26-29, retrosplenial cortex (RSC); BA 23, ventral posterior cingulate cortex; BA 28 and 34, ventral and dorsal entorhinal cortex.

ROI	PiB	HA	PiB × HA
Splenium	0.1218	0.1531	**0.0026***
Brodmann 23	0.4588	**0.0242**	**0.0257**
Brodmann 26-29	0.0840	0.4491	**0.0359**
Brodmann 28	0.7362	0.6760	0.7259
Brodmann 34	0.1158	0.0508	0.0668
Hippocampus	**0.0170**	0.2073	0.1525